RSC Advances

This article can be cited before page numbers have been issued, to do this please use: X. Zhou, X. Zhang, Z. Bao, X. Tao, H. sun and W. chen, *RSC Adv.*, 2014, DOI: 10.1039/C4RA11155A.

ROYAL SOCIETY OF CHEMISTRY

www.rsc.org/advances

View Article Online
DOI: 10.1039/C4RA11155A

Journal Name

RSCPublishing

ARTICLE

Sn-Doped TiO_2 Nanorod Arrays and Application in Perovskite Solar Cell

Cite this: DOI: 10.1039/xoxxoooooox

Xiang Zhang,‡ Zhongqiu Bao,‡ Xiyun Tao, Hongxia Sun, Wen Chen, Xingfu Zhou*

Received ooth January 2012,
Accepted ooth January 2012

DOI: 10.1039/xoxxoooooox

www.rsc.org/

Tin-doped (Sn-doped) TiO_2 nanorods arrays were successfully synthesized on TiO_2 seed layer via a mild one-pot hydrothermal method. Sn-doped TiO_2 nanorod with high electron mobility was assembled into a solid perovskite solar cell. Study indicated that the introduction of Sn element lead to the change of TiO_2 band gap from 3.0 to 3.04 eV. Electrochemical impedance spectroscopy showed that the resistance of device based on Sn-doped TiO_2 nanorod was lower than that of the undoped device. The PCE of Sn-doped perovskite device achieved 6.31%, which was almost 67% higher than that of the undoped samples.

Introduction

Recently, extensive research efforts have been devoted to the study of perovskite solar cells because of high photovoltaic efficiency, improved stability, and low cost of fabrication.[1, 2] Perovskite solar cells is based on Ag or Au layer, mesoporous[3-9]/one-dimension[10-12] metal-oxide (TiO_2[3,4,10,11], Al_2O_3[5, 6], ZnO[7, 8,12], ZrO_2[9] etc) scaffold, organo-metal halide[3, 13] perovskite ($(RNH_3)BM_3$, R=C_nH_{2n+1}[4, 14, 15], etc; B = Pb[16, 10], Sn[15]; M = Cl[6], Br[17, 18], I[13, 16]) light harvester and hole transport materials (HTM) [19,20]. PCE of 19.3% was reported for the perovskite solar cell in low-temperature processed solar cells.[21] If a perovskite solar cell provides a high open-circuit voltage (V_{oc}) of exceeding 1 V, it is possible to achieve a PCE of 20%, which indicates that organo-metal halide perovskite is extremely promising solar cell material.[22]

The organo-metal halide perovskite possesses a direct band gap, high carrier mobility, and a large absorption coefficient. [23, 24] These properties render them very attractive for use as light harvesters in perovskite solar cell.[25,26] TiO_2 as representative photoanode was usually utilized in perovskite solar cell. 1-D TiO_2 nanomaterials have been studied as an alternative to particulate nanomaterials in mesoscopic solar cell due to their superior charge transport. According to the literature,[10, 27] the electron transport and recombination in case of TiO_2 nanorod and nanotube is better than TiO_2 particles in DSSC. It is expected that perovskite materials with high extinction coefficient will provide an opportunity to fully use the superior transport properties of the 1D material. Liu synthesized single-crystalline rutile TiO_2 nanorods on transparent and conductive fluorine-doped tin oxide (FTO) glass substrates by a facile hydrothermal method[28]. Park et al[10] employ $CH_3NH_3PbI_3$ sensitized rutile TiO_2 nanorod array and a PCE of 9.4% was obtained. Whereas, Yuan et al[11] got a PCE 6.5% using freestanding TiO_2 nanotube array as scaffold. Li et al[29] used Nb doping to improve charge transport in rutile TiO_2 nanorods perovskite solar cell, he pointed out that the enhanced charge transport and understanding of electron transport property in 1D material provide the opportunity to adopt 1-D nanomaterials in thick layer perovskite solar cells. In general, metal[30,31] or nonmetal[32] elements are doped into TiO_2 to change the material properties and then to improve the PCE of solar cell. Introduction of various elements into TiO_2 lattice can also help to achieve remarkable improvements in the visible light region.[33]

Herein, we successfully prepared Sn-doped TiO_2 nanorods array. The introduction of Sn changed the band gap of TiO_2 from 3.0 eV to 3.04 eV, the diffuse reflectance spectrum of Sn-doped TiO_2 was higher than nondoped TiO_2 in visible area from 420 to 700 nm. Sn-doped TiO_2 nanorod was employed in a perovskite solar cell. The PCE of Sn-doped device yielded the value of 6.31%, which was almost 67% higher than that of nondoped TiO_2 nanorod (3.78%). Analysis of the result of the EIS revealed that the resistance of device based on Sn-doped TiO_2 nanorod was lower than that of nondoped TiO_2 nanorod. FESEM was used to investigate the morphology of the prepared Sn-doped TiO_2 and the solid state solar cell device.

Results and discussion

Sn-doped TiO_2 nanorods array is shown in Fig. 1. Fig. 1A shows that the length and width of Sn-doped nanorod are about 600 nm and 70 nm, respectively. However, the length and width of nondoped TiO_2 nanorod is about 550 nm and 100 nm, respectively (Fig. S1). Fig.1A exhibits orderly aligned arrays of nanorod with uniformity in the length and the width. Fig. 1B shows $CH_3NH_3PbI_3$-deposited TiO_2 nanorod. A mass of perovskite appears on the top and in the gaps of nanorods

which act as a light harvester. Apparently, the perovskite does not completely fill the spaces between nanorods, which are just beneficial for the penetration of HTM solution for obtaining high photovoltaic performance. Fig. 1C demonstrates the infiltration of HTM into the top and in between the gaps of TiO_2 nanorods. The Ag layer was deposited on the top of HTM and the thickness is about 80 nm.

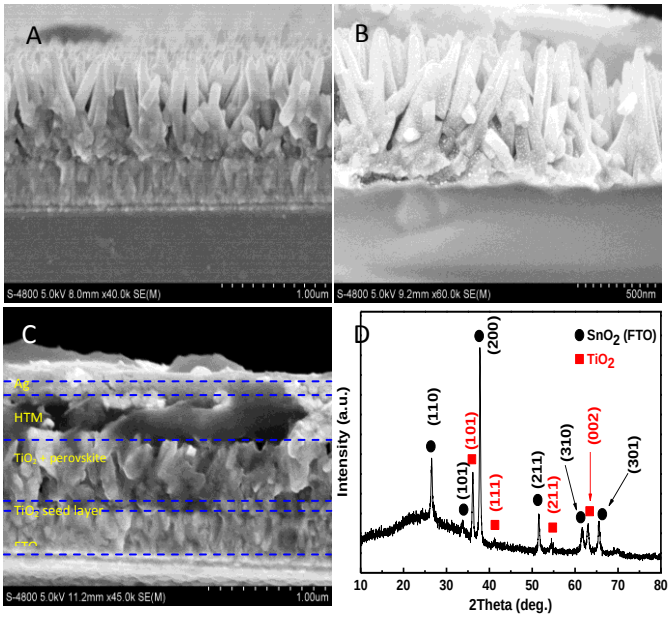

Fig. 1 Cross-sectional FESEM images of (A) Sn-doped TiO_2 nanorod grown on FTO substrate, (B) perovskite-sensitized Sn-doped TiO_2 nanorod, (C) full cell; and (D) XRD as a function of 2-theta for the Sn-doped TiO_2 nanorod.

XRD spectrum in Fig. 1D shows vertically oriented Sn-doped TiO_2 nanorod grown on FTO substrate. Except peaks of SnO_2 (FTO), the other diffraction peaks coincide with the rutile TiO_2 phase based on JCPDS 21-1276 standard card. Fig.1D shows that the (101) diffraction peak intensity of rutile TiO_2 is the highest of the other diffraction peaks, which is similar to the results obtained by Kim et al.[34,35,36] Moreover, the (002) diffraction peak intensity is relatively enhanced compared to the standard card of rutile TiO_2. The strongest intensity (101) peak reflects that the rutile TiO_2 crystal grows with (101) plane parallel to the glass substrate.

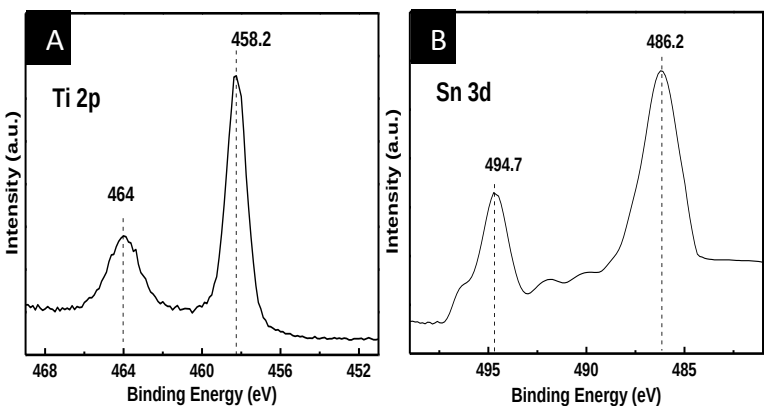

Fig. 2 XPS spectra of (A) Ti and (B) Sn in Sn-doped TiO_2 nanorod.

X-ray photoelectron spectroscopy (XPS) was performed to confirm the existence and the chemical state of elements. Fig.2A shows the Ti 2p XPS spectra of the Sn-doped TiO_2 nanorod. Compared to standard binding energy of TiO_2, these two peaks of Ti 2p spectra reveal a slight positive shift, which is attributed to the interaction among Ti, Sn, and O atoms[37]. Moreover, the Sn 3d spectra of Sn-doped TiO_2 nanorod shows a negative shift of 0.1 eV toward lower binding energy compared to the standard SnO_2, which is likely boil down to the variation in electronegativity of the Ti and Sn elements (Ti = 1.54, Sn = 1.96)[38]. These changes confirm the formation of Ti-O-Sn structure in the Sn-doped TiO_2 nanorod owing to the substitution of Ti^{4+} by Sn^{4+}.

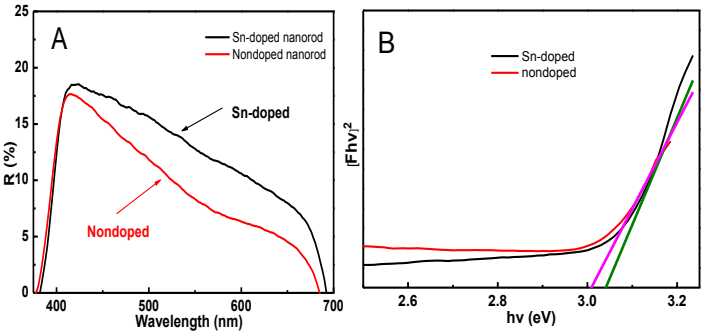

Fig. 3 (A) UV-Vis diffuses reflectance spectra of TiO_2 nanorods with and without Sn doping and (B) the corresponding optical bandgaps by Tauc plot.

Fig. 3A shows UV-Vis diffuse reflectance spectra of TiO_2 nanorod with and without Sn doping. The reflectance spectrum of Sn-doped TiO_2 nanorod is higher than that of nondoped TiO_2 nanorod from 420 to 700 nm. The optical band gaps were directly obtained from the point of the extrapolation of the linear part that meeting the abscissa of Tauc plot and shown in Fig. 3B, which showed a band gap increase from 3.0 eV to 3.04 eV. The subtle change in the band gap may attribute to the substitution of Ti^{4+} by Sn^{4+}.

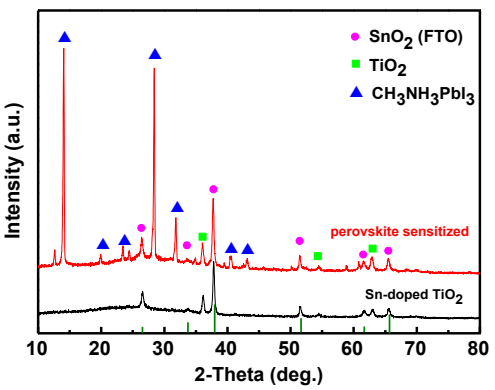

Fig.4 XRD for Sn-doped TiO_2 nanorod and perovskite sensitized Sn-doped TiO_2 nanorod grown on FTO glass.

XRD diffraction spectrum in Fig. 4 shows vertically oriented Sn-doped TiO_2 nanorod and $CH_3NH_3PbI_3$ deposited Sn-doped TiO_2 nanorod grown on FTO glass.[34,35] In Fig. 4, the diffraction peaks marked with green squares represent the rutile TiO_2 peaks and the peaks marked with magenta circles represent SnO_2 (FTO) diffraction peaks. Other diffraction peaks correspond to the tetragonal phase $CH_3NH_3PbI_3$. This indicates

View Article Online
DOI: 10.1039/C4RA11155A
ARTICLE

the successful preparation of $CH_3NH_3PbI_3$ by the consumption of PbI_2.[10]

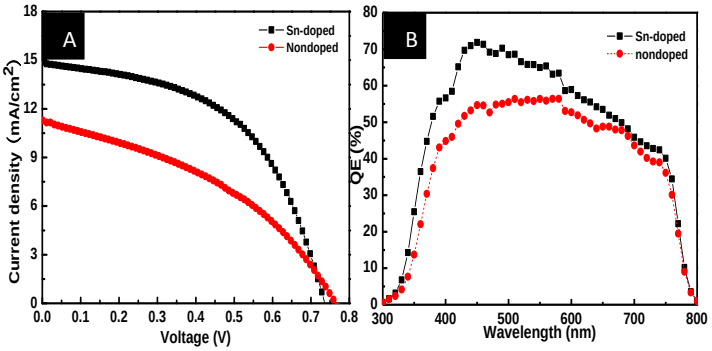

Fig. 5 Current density-voltage (I-V) curve of perovskite solar cell based on TiO_2 nanorod with and without Sn doping. (B) The external quantum efficiency of these two devices (black line: Sn-doped, red line: nondoped).

Table 1 The values of the open-circuit voltage (V_{oc}), short-circuit current density (J_{sc}), fill factor (FF) and overall conversion efficiency (η) for perovskite solar cell with Sn-doped and nondoped TiO_2 nanorod.

TiO_2	J_{sc} (mA/cm^2)	V_{oc} (V)	FF (%)	η (%)	$EQE_{(max)}$
Sn-doped	14.88	0.74	52	6.31	70%(450nm)
Nondoped	11.26	0.76	40	3.78	56%(570nm)

Fig.5 shows the results of photoelectronic performance of doped and undoped TiO_2 nanorods based solar cell. The perovskite solar cell based on Sn-doped TiO_2 shows a remarkable improvement in photocurrent density and fill factor when compared to nondoped TiO_2 (Fig. 5A and Table 1). Perovskite solar cell based on Sn-doped TiO_2 nanorod demonstrates short-circuit current density (J_{sc}) of 14.88 mA·cm^{-2}, open-circuit voltage (V_{oc}) of 0.74 V, fill factor (FF) of 0.52 and PCE of 6.31%. Thus, the higher efficiency was observed for Sn-doped TiO_2. Although V_{oc} of Sn-doped TiO_2 reduced slightly (0.02 V), J_{sc} significantly increased from 11.26 mA/cm^2 to 14.88 mA/cm^2, and the FF was also improved (12% increase) for the Sn-doped TiO_2 nanorod. Therefore, the PCE was improved from 3.78 to 6.31%. The external quantum efficiency (EQE) for the Sn-doped device achieving 6.31% PCE is shown in Fig. 5B (black line). The device shows higher EQE, the value of the maximum peak exceed 70%, however, the maximum peak value of nondoped TiO_2 is only 56%.

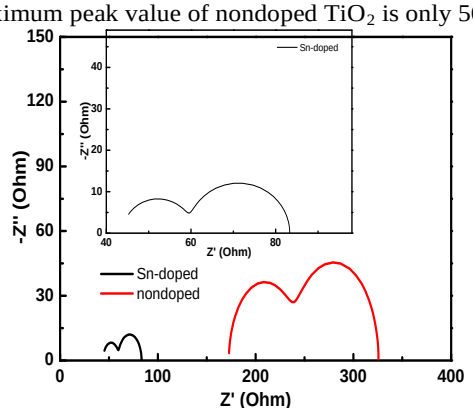

Fig. 6 Nyquist plots of perovskite solid-state device (black for Sn-doped and red for nondoped).

Evaluation of the EIS results helps to understand the success and failure of the device. Less internal impedance in cell suggests that the electronic transfer resistance is smaller; therefore, transport and extraction are easier. In contrast, higher value of internal impedance indicates higher electronic transfer resistance which prevents the electronic transport. Nyquist plots of two cells based on Sn-doped TiO_2 nanorod and nondoped nanorod are shown in Fig. 6. The test frequency was from 1 to 100 KHz, amplitude of 5 mV. The high frequency semicircle is due to hole transport and extraction in the cathode, which represents the transport and extraction of hole and the corresponding capacitance between the interface of HTM and Ag layer. Comparison of the Sn-doped and nondoped (Fig. 6) devices reveals that the transport resistance of device based on Sn-doped TiO_2 nanorod is smaller than that of the nondoped TiO_2 nanorod. Small transport resistance is beneficial for the hole transfer[39]. The semicircle in the middle frequency represents the synergistic effect of the recombination resistance of electron and hole and the chemical capacitance of films. Simultaneously, the series resistance (R_s) of these two cells was also observed. The value of R_s is the point of intersection between the semicircle and the X-axis in the high frequency section. The value of R_s is less than 45 Ω for the Sn-doped TiO_2 nanorod device as shown in the inset of Fig.6. However, for the nondoped device, the value of R_s increases to 170 Ω. Other sources can also contribute the improved photoelectric activity. For example, the potential difference between TiO_2 and SnO_2 allows electrons to easily migrate from the TiO_2 surfaces to the SnO_2 conduction band, which lead to decrease in the radiation combination of photoinduced electrons on the TiO_2 surfaces[40]. In addition, the possible formation of $Sn_xTi_{1-x}O_2$at the interface and associated modulation of electronic properties also facilitates the electron transport through TiO_2 interfaces[41].

Conclusions

Sn-doped TiO_2 nanorod was successfully fabricated on a FTO substrate via a mild one-pot hydrothermal method. Doping of Sn changed the band gap of TiO_2 material and enhances the light utilization and capture, which improved the reflectance between 420 to 700 nm. Sn-doped TiO_2 nanorod was utilized in a perovskite solid state cell which yielded the PCE of 6.31%. The PCE of Sn-doped (6.31%) was almost 67% higher compared to that of nondoped TiO_2 nanorod (3.78%) under the same condition. The results of EIS analysis revealed that the resistance of Sn-doped TiO_2 nanorod materials was smaller than that of nondoped TiO_2, thus explaining the higher PCE of cell based on Sn-doped TiO_2 nanorod materials.

Experimental

All the chemicals were analytical grade and used without further purification. Sn-doped TiO_2 nanorods were grown on a TiO_2 seed layer coated FTO substrates. The seed layers were grown on cleaned FTO glasses according to a procedure reported in the literature.[32] The seed layer coated substrates were used to grow the TiO_2 nanorods and to prevent direct electrical contact between FTO and HTM. Sn-doped nanorods were prepared via hydrothermal synthesis. Briefly, 20 mL hydrochloric acid (37% wt) was added into the 20 mL deionized water and stirred for about 10 min. Subsequently, Tin (Ⅳ) chloride pentahydrate ($SnCl_4$ $5H_2O$, 0.1g) was added and the contents were stirred until it was completely dissolved.

View Article Online
DOI: 10.1039/C4RA11155A

Tetrabutyl titanate (0.75 mL) was added and the mixture was further stirred for 30 min. Several pieces of FTO with seed layer were placed inside an 80 mL Teflon-lined stainless steel autoclave. The above mentioned mixed solution was then transferred into an autoclave, then, placed it into a 150 ℃ oven for 150 min. After naturally cooling, the as-formed thin film was washed with deionized water and finally dried, then calcined at 500℃ for 30min.

The perovskite sensitizer $CH_3NH_3PbI_3$ was deposited on the TiO_2 nanorod film by a two-step method following the reported procedure, Methylamine (32% in ethanol, 40.5 mL) and hydroiodic acid (57 wt% in water, 30 mL) were taken in a 250 mL flask and allowed to react in an ice bath for 2 h. Subsequently, the solvents were evaporated at 50 ℃ to produce precipitate. The precipitate was washed three times with ethyl ether and ethanol, filtrated and the product CH_3NH_3I was isolated. CH_3NH_3I solution (10 $mg{\cdot}mL^{-1}$) was prepared by dissolving CH_3NH_3I in 2-propanol, and PbI_2 solution (100 mM was prepared by dissolving PbI_2 in γ-butyrolactone at 70℃ for 2 h.

The perovskite $CH_3NH_3PbI_3$ deposition is conducted in the air with humidity around 40%. PbI_2 solution was spin-coated immediately and dried at 70 ℃ for 30 min. After cooling, the glass was placed into CH_3NH_3I solution for 30 s and the film turn into black brown color. After drying at 100℃ 15 min, spiro-OMeTAD was spin-coated at 4,000 rpm for 20s. Finally, silver (Ag) was deposited using thermally evaporated on top of the device.

The cross-sectional morphologies of Sn-doped TiO_2 and full cell were measured by a Hitachi S-4800 field emission scanning electron microscope (FESEM). The phases of the Sn-doped TiO_2 nanorod were investigated by X-ray diffraction (XRD, SmartLab, Rigaku). Photocurrent and voltage were measured by a Keithley 2400 source meter and a solar simulator (Oriel 94023A) equipped with a 450 W xenon lamp (Newport 6279NS). The output power was adjusted to match AM 1.5 global sunlight, which was calibrated by a certified reference silicon solar cell with intensity of 100 mW cm^{-2} prior to use. A black aperture mask was applied to define the active area during photocurrent and voltage measurement. EIS measurement was performed with alternating current amplitude of 5 mV over the frequency range of 1 Hz to 100 KHz. Ultraviolet-Visble (UV-Vis) spectrum measurements were conducted using a Lambda 950 spectrophotometer.

Acknowledgements

This research was supported by the Natural Science Foundation of China (No. U1162108, No. 51272104); the Natural Science Foundation of Jiangsu Province Office of Education (BK20131409), Natural Science Foundation of the Jiangsu Higher Education Institutions of China (No.11KJA150002), Qing Lan project of Jiangsu Province, the Financial Foundation of State Key Laboratory of Materials-Oriented Chemical Engineering and A Project Funded by the Priority Academic Program Development of Jiangsu Higher Education Institutions.

Notes and references

State Key Laboratory of Materials-Oriented Chemical Engineering, College of Chemistry and Chemical Engineering, Nanjing University of Technology, Nanjing 210009, PR China. *Fax: +86-25-83172270; Tel: +86-25-83172270; E-mail: zhouxf@njtech.edu.cn*

‡ These authors are co-first authors; they contributed equally to the work.

1. T.Moehl,M.Grätzel,J.E.Moser,*Nat.photonics*,2014,**8**,250.
2. J.Burschka,N.Pellet,S.J.Moon,P.Gao,M. K.Nazeeruddin, M.Grätzel, *Nature* 2013, **499**, 316.
3. H.S.Kim,C.R.Lee,J.H.Im,K.B.Lee,T.Moehl, A.Marchioro, S.J.Moon, R.Humphry-Baker,J.H.Yum, J. E.Moser,*Sci.Rep.*,2012,**2**591.
4. M.Grätzel,S.I.Seok,*Nat.photonics*,2013,**7**,487.
5. M.M.Lee,J.Teuscher,T.Miyasaka,T.N.Murakami,H.J.Snaith,*Science*, 2012,**338**,643.
6. J.M.Ball,M.M.Lee, A.Hey, H.J.Snaith, *Energ. Environ. Sci.*, 2013,**6**, 1739.
7. D. Liu, T. L. Kelly, *Nat. Photonics*, 2014, **8**, 133.
8. D.Y.Son, J.H.Im,H.S.Kim,N.G.Park,*J.Phys.Chem.C* ,2014,**118**,16567.
9. D.Bi, S.J.Moon, L.Häggman, G.Boschloo, L.Yang, E. M.Johansson, M. K.Nazeeruddin, M.Grätzel, A.Hagfeldt, *Rsc Advances* 2013, **3**, 18762.
10. H.S.Kim,J.W.Lee,N.Yantara,P.P.Boix,S.A. Kulkarni,S. Mhaisalkar,M. Gratzel, N.G.Park,*NanoLett.*,2013,**13**,2412.
11. X.Gao, J.Li, J.Baker,Y.Hou,D.Guan,J.Chen,C.Yuan, *Chem. Commun.*, 2014, **50**, 6368.
12. D.Y.Son,J.H.Im, H.S. Kim,N.G.Park,*J.Phys.Chem.C*, 2014,**118**,16567.
13. T.Baikie, Y.Fang, J. M.Kadro, M.Schreyer, F.Wei, S. G.Mhaisalkar, M.Graetzel, T. J.White, *J.Mater.Chem.A* ,2013, **1**, 5628.
14. Z.Cheng, J.Lin, *Crystengcomm* 2010, **12**, 2646.
15. F. Hao, C.C. Stoumpos, R. Chang, M. G. Kanatzidis, *J.Am.Chem.Soc.*, 2014, **136**, 8094.
16. Y.Kawamura, H.Mashiyama, K.Hasebe, *J. Phys. Soc. Japan*, 2002, **71**, 1694.
17. A.Kojima,K.Teshima,Y.Shirai,T.Miyasaka,*J.Am.Chem.Soc.*,2009,**131**, 6050.
18. E.Edri,S.Kirmayer,D.Cahen,G.Hodes, *J.Phys.Chem.Lett.*,2013,**4**, 897.
19. J.H.Heo,S. H.Im,J.H.Noh,T.N.Mandal,C.S.Lim, J.A.Chang, Y. H.Lee, H.j.Kim, A.Sarkar, M. K.Nazeeruddin,*Nat. Photonics*,2013,**7**,486.
20. J.A.Christians,;R.C.Fung,P.V.Kamat,*J.Am.Chem.Soc*.,2014,**136**,758.
21. H. Zhou,Q. Chen, G. Li, S. Luo, T. Song, H. Duan, Z.Hong,J.You,Y. Liu,Y.Yang, *Science*,2014,345,542.
22. N.G.Park, *J. Phys. Chem. Lett.* 2013, **4**, 2423.
23. A.Yella, L.P.Heiniger, P.Gao, M. K.Nazeeruddin, M.Grätzel, *Nano lett.*, 2014,**14**,2591.
24. S. Aharon, S. Gamliel, B. Cohen, L.Etgar, *Phys.Chem.Chem.Phys.*, 2014,**16**,10512.
25. S.Kazim, M. K.Nazeeruddin, M.Grätzel, S. Ahmad, *Angew. Chem. Int. Edit.*,2014,**53**,2812.
26. P.Docampo, A.Hey, S.Guldin, R.Gunning, U.Steiner, H. J.Snaith, *Adv. Funct. Mater.*,2012,**22**,5010.
27. S. H.Kang, S. H.Choi, M. S.Kang, J. Y.Kim, H.S.Kim,T.Hyeon, Y. E.Sung, *Adv. Mater.*,2008,**20**,54.
28. B.Liu, E.S.Aydil, , *J. Am. Chem. Soc.*,2009,**131**,3985.
29. M.Yang, R.Guo, K.Kadel, Y.Liu, K.Shea, R.Bone, X.Wang, J.Heand, W. Z. Li, *J. Mater. Chem. A*, 2014, DOI: 10.1039/C4TA02635G
30. C.Y.Wang,D.W.Bahnemann,J.K.Dohrmann,*Chem.Commun.*, 2000, **1.** 1539.
31. F.Coloma,F.Marquez,C.Rochester,J.Anderson,Phys.Chem.Chem.Phys. ,2000,**2**,5320.
32. X.Chen, C.Burda, *J. Am. Chem. Soc.* ,2008,**130**,5018.
33. C.Burda,Y.Lou,X.Chen,A.C.Samia,J.Stout,J.L.Gole, *Nano lett.*,2003, **3**,1049.
34. H.Pan, J.Qian, Y.Cui, H.Xie, X.Zhou, *J.Mater.Chem.*, 2012, **22**, 6002.
35. L.Liu, J.Qian, B.Li, Y.Cui, X.Zhou, X.Guo,W.Ding, *Chem.Commun.*, 2010, **46**, 2402.
36. M.Liu, L.Piao, L.Zhao, S.Ju,C.Zhou,W.Wang, *Chem. Commun.*, 2010, **46**, 1664.
37. Y. Duan, N.Fu,Q.Liu,Y.Fang,J.Zhang,Y.Lin, *J. Phys. Chem. C*, 2012, **116**, 8888.
38. J. Li, H. C. Zeng, *J. Am. Chem. Soc.*, 2007, **129**, 15839.
39. M. Thambidurai, J. Kim, H.Song, Y.Ko, N. Muthukumarasamy, D.Velauthapillai, C.Lee, *J.Mater.Chem.A*, 2014,**2,**11426.
40. Z. Liu, D. D. Sun, P. Guo, J. O. Leckie, *Nano Lett.* 2007,**7**,1081.
41. J. Pan, S. M. Huhne, H. Shen, L. S.; Xiao, P. Born, W. Mader, S. J. Mathur, *J. Phys. Chem. C* 2011, **115,** 17265.